

Interlayer Structure and Dynamics of Cl^- – LiAl_2 -Layered Double Hydroxide: ^{35}Cl NMR Observations and Molecular Dynamics Modeling

Xiaoqiang Hou,* Andrey G. Kalinichev, and R. James Kirkpatrick

Department of Geology, University of Illinois at Urbana–Champaign, Urbana, Illinois, 61801

Received August 8, 2001. Revised Manuscript Received January 16, 2002

^{35}Cl NMR experiments and molecular dynamics modeling provide significant new insight into the structure and dynamics of the interlayer species in the layered double hydroxide (LDH) $\text{LiAl}_2(\text{OH})_6\text{Cl}\cdot n\text{H}_2\text{O}$. The LiAl_2 LDHs have wide ranging potential applications as catalysts, as filtration and exchange materials, and in drug and gene-therapy delivery systems, and many of these applications depend on the behavior of interlayer species. Room-temperature MAS and static ^{35}Cl NMR data indicate that the Cl^- environments vary significantly with hydration state. The fully hydrated paste form has three types of Cl^- : surface Cl^- that yields a sharp solution-like peak at 0 ppm, interlayer Cl^- that yields a resonance dominated by uniaxial chemical shift anisotropy (CSA), and interlayer Cl^- that yields a structureless peak that is not fully narrowed by MAS. The relative abundance of the CSA dominated peak increases with decreasing hydration and is the only resonance observed for fully dried samples. For the dehydrated samples, this resonance corresponds to the one Cl^- site in the crystal structure. Both types of interlayer $^{35}\text{Cl}^-$ sites are present for paste and partially hydrated samples, and comparison to the results of molecular dynamics modeling suggests that the CSA-dominated resonance is due to Cl^- on two types of prism sites with time averaged uniaxial symmetry and that the structureless peak is due to Cl^- on dynamically averaged sites stabilized by H-bonding from both OH groups and interlayer waters. Variable-temperature NMR experiments show a disordered, static interlayer at $-90\text{ }^\circ\text{C}$. With increasing temperature, surface Cl^- has observable dynamical motion at $-60\text{ }^\circ\text{C}$, whereas appreciable motion in the interlayer does not begin until above $-30\text{ }^\circ\text{C}$. At $70\text{ }^\circ\text{C}$, signal for the two types of interlayer sites is nearly fully averaged, indicating site exchange at frequencies of at least 10^3 Hz . This observation is consistent with relatively rapid site hopping observed in the MD simulations. The simulations also demonstrate the presence of hopping libration of the interlayer water molecules, as previously observed for other LDH compounds, provide important insight into the structure of the interlayer H-bonding network, and provide structural understanding of the smaller interlayer water content of the LiAl_2 LDH phases compared to the Ca_2Al and $\text{Mg}_{3-x}\text{Al}_x$ phases.

Introduction

Layered double hydroxides are unique among inorganic layer-structure materials in having permanent, positive layer charges, significant anion-exchange capacities and large surface areas.¹ Because of these unique properties, they have wide ranging potential applications as catalysts,¹ as filtration and exchange materials,² and in drug and gene-therapy delivery systems.³ Many of these applications depend on the behavior of interlayer and surface water and anions, and understanding the molecular-scale structure and dynamics of the interlayer and surface species is central to advancing their application.^{4–9} The study reported here focuses on the structural order and dynamics of

interlayer chloride in the compound $\text{LiAl}_2(\text{OH})_6\text{Cl}\cdot n\text{H}_2\text{O}$. Our previous experimental and computational studies have focused on the behavior of interlayer and surface Cl^- , SeO_4^{2-} , SeO_3^{2-} , and NO_3^- in related Mg_2Al and Ca_2Al compounds^{4–8} and on the thermal decomposition behavior of $\text{LiAl}_2(\text{OH})_6\text{Cl}\cdot n\text{H}_2\text{O}$.¹⁰ Many other species have also been investigated.^{11–14}

LDH crystal structures consist of positively charged hydroxide sheets separated by interlayers containing exchangeable anions and water molecules.^{1,15} In the

(4) Kirkpatrick, R. J.; Yu, P.; Hou, X.-Q.; Kim, Y. *Am. Mineral.* **1999**, 84, 1186.

(5) Hou, X.-Q.; Kirkpatrick, R. J.; Yu, P.; Moore, D.; Kim, Y. *Am. Mineral.* **2000**, 85, 173.

(6) Hou, X.-Q.; Kirkpatrick, R. J. *Chem. Mater.* **2000**, 12, 1890–1897.

(7) Kalinichev, A. G.; Kirkpatrick, R. J.; Cygan, R. T. *Am. Mineral.* **2000**, 85, 1046–1052.

(8) Wang, J.-W.; Kalinichev, A. G.; Kirkpatrick, R. J.; Hou, X.-Q. *Chem. Mater.* **2001**, 13, 145–150.

(9) Isupov, V. P.; Gabuda, S. P.; Kozlova, S. G.; Chupakhina, L. C. *J. Struct. Chem.* **1998**, 39, 362–366.

* Corresponding author. Telephone: (217) 244-2355. Fax: (217) 244-4996. E-mail: xhou@uiuc.edu.

(1) Cavani, F.; Trifiro, F.; Vaccari, A. *Catal. Today* **1991**, 11, 173.

(2) Bish, D. L. *Bull. Mineral.* **1980**, 103, 170–175.

(3) Choy, J.-H.; Kwak, S.-Y.; Park, J.-S.; Jeong, Y.-J.; Portier, J. J. *Am. Chem. Soc.* **1999**, 121, 1399–1400.

LiAl₂ compounds, Li⁺ occupies the octahedral vacancies of a dioctahedral gibbsite sheet,^{9,16,17} and on the basis of X-ray diffraction (XRD) data, the Li/Al distribution is highly ordered.^{16,17} XRD, however, provides limited information about the local structural environments and dynamical behavior of interlayer and surface species. ⁷Li and ²⁷Al NMR data of LiAl₂(OH)₆Cl⁻·*n*H₂O have been reported to address the Li/Al structure at atomic scale.⁹ The ³⁵Cl nuclear magnetic resonance (NMR) data reported here provides otherwise unobtainable information about the interlayer and surface species and adds greatly to understanding of their structural environments and dynamics. NMR is an element-specific, direct probe of local structure and dynamics, and ³⁵Cl NMR of chloride ion is particularly useful for investigating the interlayer due to its high sensitivity to nearest neighbor structure, its relatively high abundance and its moderate quadrupole moment.⁴ Parallel molecular dynamics modeling provides structural and dynamical insight that substantially improves interpretation of the NMR data.^{7,8}

Our previous study of LiAl₂(OH)₆Cl⁻·*n*H₂O¹⁰ focuses on its thermal decomposition and structural evolution in the temperature range 20–1100 °C. Here we examine the dependence of interlayer Cl⁻ structure and dynamics with progressive drying from a fully hydrated paste state to full dehydration at room temperature and with variable temperature from -90 to +90 °C. Compositional analyses, thermogravimetry, differential scanning calorimetry, powder XRD, and ²⁷Al, ^{6,7}Li and ³⁵Cl NMR data for the starting materials and heated samples are reported in the first paper¹⁰ and will not be duplicated here. Key conclusions of this work relevant here include the following. (1) The Al/Li molar ratios of the LDH samples are close to 2, independent of the Al/Li ratio of the aqueous solution from which they precipitated, and the octahedral Al, Li distribution is highly ordered, independent of interlayer water content. (2) Dehydration (loss of surface and interlayer water molecules) begins near room temperature, depending on the relative humidity, and culminates near 125 °C. (3) Decomposition (dehydroxylation) begins at about 300 °C. The results of the current study confirm a high degree of interlayer Cl⁻ order in the dehydrated compound, less interlayer order in the hydrated compound and significant structural and dynamical changes with varying relative humidity (RH) and temperature.

Experiment and Computation

Three samples, identified as LiAlCl5, LiAlCl6, and LiAlCl8, were prepared using a direct precipitation method.¹⁰ Their chemical compositions are as follows.

- (10) Hou, X.-Q.; Kirkpatrick, R. J. *Inorg. Chem.* **2001**, *40*, 6397–6404.
- (11) van der Pol, A.; Mojet, B. L.; van de Ven, E.; de Boer, E. J. *Phys. Chem.* **1994**, *98*, 4050–4054.
- (12) Boclair, J. W.; Braterman, P. S. *Chem. Mater.* **1999**, *11*, 298–302.
- (13) Zeng, H. C.; Xu, Z. P.; Qian, M. *Chem. Mater.* **1998**, *10*, 2277–2283.
- (14) Hou, X.-Q.; Kirkpatrick, R. J. *Chem. Mater.* **2002**, *14*, 1195–1200.
- (15) Terzis, A.; Filippakis, S.; Kuzel, H. J.; Burzlaff, H. Z. *Kristallogr.* **1987**, *181*, 29.
- (16) Serna, C. J.; Rendon, J. L.; Iglesias, J. E. *Clays Clay Miner.* **1982**, *30* (3), 180–184.
- (17) Bessergueney, A. V.; Fogg, A. M.; Francis, R. J.; Price, S. J.; O'Hare, D.; Isupov, V. P.; Tolochko, B. P. *Chem. Mater.* **1997**, *9*, 241–247.

LiAlCl5: Li_{0.890}Al_{2.110}(OH)₆Cl_{0.748}(CO₃)_{0.057}·0.503H₂O.

LiAlCl6: Li_{0.949}Al_{2.049}Fe_{0.002}(OH)₆Cl_{0.922}(CO₃)_{0.030}·0.866H₂O

LiAlCl8: Li_{0.970}Al_{2.030}(OH)₆Cl_{0.977}·0.644H₂O

Most of the data reported here is for sample LiAlCl5, but sample LiAlCl6 was used for some rehydration experiments and sample LiAlCl8 for supplemental variable relative humidity (RH) data collected at *H*₀ = 17.6 T. Specimens examined include newly made paste; aliquots dried at room temperature (room temperature)/room humidity (ca. 35%), over P₂O₅ at room temperature (0% RH), and in air at temperatures up to 200 °C; aliquots heated at 70 °C and equilibrated over RH salt buffers;¹⁸ and pastes made from DI water and aliquots previously dried at 70 °C. Quantitative determination of the interlayer Cl⁻/H₂O ratio under the different drying conditions has not been attempted due to the difficulties of separating surface and interlayer water in TGA measurements.

Static and MAS ³⁵Cl NMR spectra were collected using both a Varian INOVA 750 spectrometer (*H*₀ = 17.62 T, *v*₀ = 73.4 MHz) and a home-built 500 MHz spectrometer (*H*₀ = 11.74 T, *v*₀ = 48.9 MHz) equipped with a Tecmag Aries data system. Spectra from both spectrometers were obtained with Doty Scientific fast MAS probes. Static spectra were collected using a 90°-τ-180° echo pulse sequence, and MAS spectra were collected using a single pulse sequence with 16-step phase cycling. For spectra collected at room temperature and controlled RH, the samples were placed in open containers in a sealed desiccator or glovebag, equilibrated for at least 1 week over saturated salt buffers, and quickly loaded into glass tubes (or MAS rotors) and sealed with epoxy or rotor caps just prior to data collection. Preheated samples were also quickly loaded just prior to data collection to avoid moisture absorption. In situ variable-temperature spectra (LiAlCl5) were collected from +90 to -90 °C using a liquid nitrogen cooling system and a resistance heating system. NaCl (1 M) aqueous solution was used as the external chemical shift standard and its chemical shift was set at 0 ppm.⁴ Typically, recycle times of 1 s were used.

Molecular dynamics (MD) simulations were performed using the Cerius² molecular modeling software package.¹⁹ The details of the simulations are similar to our previous publications.^{7,8} The initial structures for the simulations of the hydrated and dehydrated phases of Cl⁻-LiAl₂ were based on those observed experimentally.¹⁷ Each simulated supercell contained 4 × 4 × 1 crystallographic unit cells, resulting in total of 32 Cl⁻ ions distributed equally between two statistically equivalent interlayers. Additionally, 32 water molecules were equally distributed between the two interlayers of the hydrated phase. Except for the periodic boundary conditions,¹⁹ there were no additional symmetry constraints. The simulated structures were treated as triclinic (*P*1 symmetry) and all cell parameters, *a*, *b*, *c*, *α*, *β*, and *γ*, were considered independent variables during the simulations. Each atom in the system had a partial charge, and the total potential energy of the simulated system consisted of a Coulombic term representing the sum of all electrostatic interactions between partial atomic charges and a Lennard-Jones (12–6) term modeling the short-range van der Waals interactions:

$$U = \sum_{i,j} \left\{ \frac{q_i q_j}{4\pi\epsilon_0 r_{ij}} + 4\epsilon_{ij} \left[\left(\frac{\sigma_{ij}}{r_{ij}} \right)^{12} - \left(\frac{\sigma_{ij}}{r_{ij}} \right)^6 \right] \right\} \quad (1)$$

where *r*_{ij} is the distance between atoms *i* and *j*, *q*_{*i*} and *q*_{*j*} are partial charges centered on these atoms, ϵ_{ij} and σ_{ij} are parameters of the Lennard-Jones interaction potential, and ϵ_0 is the dielectric permittivity of vacuum ($\epsilon_0 = 8.85419 \times 10^{-12}$ F/m). The Lennard-Jones parameters of unlike interactions

(18) Lide, D. R. *CRC Handbook of Chemistry and Physics*, 79th ed.; CRC Press: Boca Raton, FL, 1998.

(19) Molecular Simulations Inc. *Cerius2-4.0 User Guide. Forcefield-Based Simulations*; MSI: San Diego, CA, 1999.

Table 1. Potential Parameters Used in MD Simulations of Cl⁻-LiAl₂ LDH

	$\sigma_{ii}/\text{\AA}$	$\epsilon_{ii}/(\text{kJ/mol})$	Q_i/e
Al ^a	4.271	5.56×10^{-6}	+1.575
O(hydroxide) ^a	3.166	0.650	-0.95
H(hydroxide) ^a			+0.425
H(water) ^b			+0.41
O(water) ^b	3.166	0.650	-0.82
Li ⁺ ^c	1.508	0.690	+1.0
Cl ⁻ ^d	4.400	0.418	-1.0

^a Reference 20. ^b Reference 22. ^c Reference 23. ^d Reference 24.

were calculated according to the “arithmetic” combining rules:

$$\sigma_{ij} = \frac{\sigma_{ii} + \sigma_{jj}}{2}; \quad \epsilon_{ij} = \sqrt{\epsilon_{ii}\epsilon_{jj}} \quad (2)$$

A “spline cut-off” method was used to treat the non-Coulomb interactions, and all long-range electrostatic interactions were treated using the Ewald summation method.¹⁹ The specific potential parameters used in the present simulations are given in Table 1. General details of the force field parametrization are reported elsewhere.²⁰ For water, the flexible version²¹ of the simple point charge (SPC) interaction potential²² was used. Lennard-Jones terms centered on the O atoms were assumed equivalent for both H₂O molecules and the oxygens of the OH groups of the hydroxide layers, while those centered on the H atoms were ignored. The total energy of each model was minimized before starting the MD simulations. These optimized models were then used as initial configurations for *NPT*-ensemble MD simulations performed at 1 bar and 300 K using the Parrinello–Rahman²³ isothermal–isobaric MD algorithm. A time step of 0.001 ps was used to integrate the equations of motion, and the dynamic trajectories of each atom in the system were recorded for further analysis every 0.01 ps over the 100 ps equilibrium period of each simulation, which was preceded by a preequilibration MD run of approximately the same length.

Results and Spectral Interpretation

Room Temperature ³⁵Cl NMR. The room temperature ³⁵Cl NMR spectra vary significantly depending on sample treatment (Figure 1, samples LiAlCl₅ and LiAlCl₆, see caption) and indicate that interlayer Cl⁻ undergoes progressive transition from a well-ordered structural arrangement to a highly disordered arrangement with increasing interlayer hydration. Three components can be identified based on analysis of the entire set of data: a small narrow component near 0 ppm (e.g., Figure 1a), a component that is well simulated with uniaxial chemical shift anisotropy (CSA; e.g., Figure 1, parts e and f), and a nearly structureless component which is present for samples that have not been fully dried (e.g., Figure 1, parts a–d). The narrow component near 0 ppm is present for only the paste sample. On the basis of our previous work^{4,5} it is readily assigned to surface Cl⁻ undergoing rapid, isotropic exchange with the solution. This surface Cl⁻ is not removed during washing due to electrostatic attraction to the solid. It

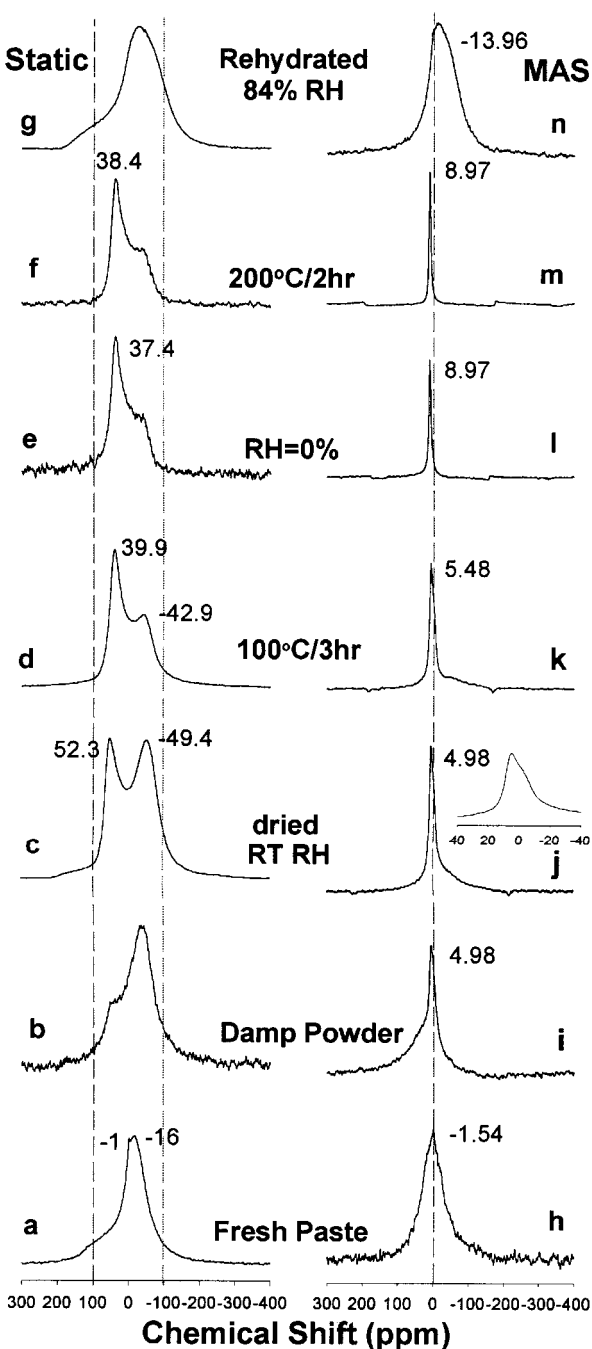


Figure 1. Static and MAS ³⁵Cl NMR spectra of LiAl₂(OH)₆-Cl·nH₂O treated under the conditions indicated. Data were collected at $H_0 = 11.7$ T. All spectra are for the sample LiAlCl₅ except that parts g and n are for the sample LiAlCl₆. The inset in spectrum j is the same spectrum, but the horizontal scale is much expanded to highlight the quadrupolar contribution to the line shape. See text for details.

is needed for electrostatic charge neutrality, but it is able to exchange with solution-like sites near the surface. The other two components are assigned to interlayer Cl⁻.

The second component is present for all samples, is dominated by CSA, and contains little second-order quadrupolar contribution. For the fully dehydrated samples (RH = 0% and heated at 200 °C, Figure 1, parts e and f), it is the only component present. This resonance collapses to a narrow, symmetrical peak under MAS (Figure 1, parts l and m), and the singularities in

(20) Cygan, R. T.; Liang, J.; Kalinichev, A. G. *J. Phys. Chem. B* **2002**, manuscript in preparation.

(21) Teleman, O.; Jönsson, B.; Engström, S. *Mol. Phys.* **1987**, *60*, 193.

(22) Berendsen, H. J. C.; Postma, J. P. M.; van Gunsteren, W. F.; Hermans, J. In *Intermolecular Forces*; Pullman, B., Ed.; Riedel: Dordrecht, The Netherlands, 1981; p.331.

(23) Dang, L. X. *J. Chem. Phys.* **1992**, *96*, 6970.

(24) Smith, D. E.; Dang, L. X. *J. Chem. Phys.* **1994**, *100*, 3757.

(25) Parrinello, M.; Rahman, A. *J. Appl. Phys.* **1981**, *52*, 7182.

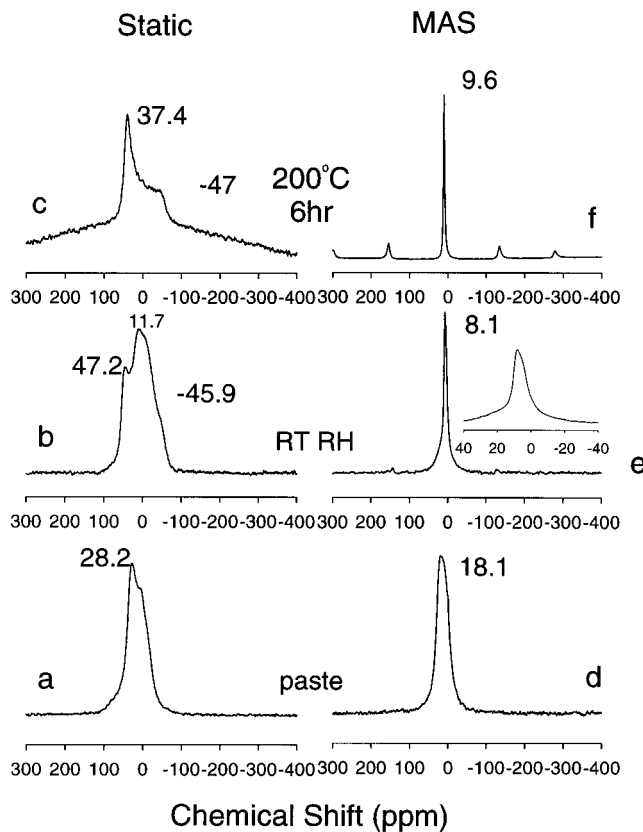


Figure 2. Static and MAS ^{35}Cl NMR spectra of $\text{LiAl}_2(\text{OH})_6\text{-Cl}\cdot n\text{H}_2\text{O}$ treated under the conditions indicated. Data collected at $H_0 = 17.6$ T. All spectra are for the sample LiAlCl8. The inset in spectrum e is the same spectrum, but the horizontal scale is much expanded to highlight the quadrupolar contribution to the line shape. See text for details.

the static spectra are independent of H_0 field (Figures 1e,f and 2c). Thus, there is little quadrupolar contribution to its peak shape. The CSA pattern is well-defined for these dehydrated samples, which are expected to have highly ordered interlayer Cl^- ,¹⁷ and the simulated $\delta_{\perp} = 44$ ppm, $\delta_{\parallel} = -60$ ppm, and $\delta_i = 9.3$ ppm. The MAS peak maxima for these samples are at 8.97 ppm, in excellent agreement with the simulated δ_i . This single resonance corresponds to the one ordered Cl^- position in dehydrated $\text{LiAl}_2(\text{OH})_6\text{Cl}$.¹⁷ In this dehydrated phase, the interlayer Cl^- is located at the center of the interlayer along the *c*-axis (see Figure 5c) and directly above and below Li in the gibbsite sheet. It forms linear $\text{Cl}\cdots\text{OH}\cdots\text{Li}\cdots\text{OH}\cdots\text{Cl}$ chains perpendicular to the hydroxide layers,¹⁷ and this arrangement is fully consistent with the observed uniaxial ^{35}Cl CSA pattern.

The relative intensity of this CSA-dominated component decreases with increasing hydration. Simulations of the static spectra yield relative intensities for it of 0.23 for the paste (Figure 1a), 0.35 for the damp powder (Figure 1b), 0.64 for the room dried sample (Figure 1c), and 0.89 for the 100 °C heated sample (Figure 1d). It also becomes less well-defined and broader with increasing hydration. For the room temperature and room humidity spectrum (Figure 1c), it can be well simulated with $\delta_{\perp} = 59$ ppm, $\delta_{\parallel} = -102$ ppm, $\delta_i = 5.3$ ppm. The MAS peak maximum for this sample is 4.98 ppm, but under MAS its resonances for this and the other incompletely dehydrated samples (Figure 1i,j,k) are not symmetric and contain some unaveraged second-order

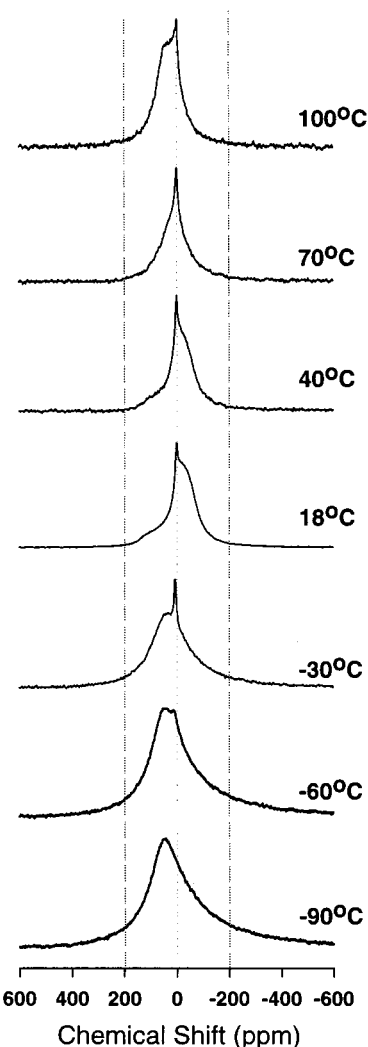


Figure 3. Static ^{35}Cl NMR spectra of a paste sample of $\text{LiAl}_2(\text{OH})_6\text{Cl}\cdot n\text{H}_2\text{O}$ (LiAlCl5) collected at the indicated in situ temperatures at $H_0 = 11.7$ T.

quadrupolar contribution (see the inset of Figure 1j). For the room humidity sample, simulation of the MAS spectrum yields $\delta_i = 11$ ppm, a quadrupole coupling constant (QCC) = 0.9 MHz and a quadrupolar asymmetry parameter (η) = 0. Peak narrowing and shifting of the peak maximum to more positive values at higher field (Figure 2e) confirm the presence of a quadrupolar effect. This quadrupolar effect together with such structural factors as the presence or absence of water molecules between interlayer Cl^- ions and site disorder may shift the CSA singularities of the incompletely dehydrated samples. For the freshly made paste (Figure 1a), this component is broad and ill-defined.

In parallel, the relative intensity of the structureless component increases with increasing hydration (Figure 1a-f). It is not observable at $\text{RH} = 0\%$ and for the 200 °C sample. In contrast, it dominates the static spectrum of the fresh paste (Figure 1a), for which it has a peak maximum of -16 ppm and a fwhh of ~85 ppm. The two components are not resolvable in the MAS spectrum of this sample (Figure 1h), and the observed MAS peak is structureless with a fwhh of ~67 ppm. In the static spectra of the damp powder (Figure 1b), the room-dried (Figure 1c) and 100 °C dried (Figure 1d) samples, this component overlaps the δ_{\parallel} singularity of the CSA

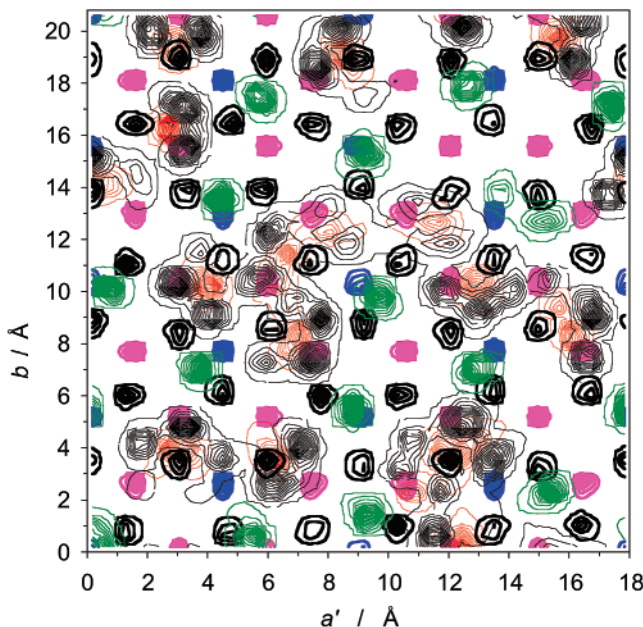


Figure 4. Contour maps of atomic probability densities in the plane of the interlayer (b , a^*) of $\text{LiAl}_2(\text{OH})_6\text{Cl}\cdot\text{H}_2\text{O}$ computed using MD methods. Contours: green = Cl^- , red = O of water, thin black = H of water, thick black = H of OH below, pink = Al of hydroxide layer below, and blue = Li of hydroxide layer below.

dominated component near -45 ppm, but it is readily visible in the MAS spectra. The similarity of the widths of this component in the MAS and static spectra indicates that it is not dominated solely by second-order quadrupolar effects and that dynamical effect and/or inhomogeneous broadening due to structural disorder may contribute.

The changes in the ^{35}Cl spectra due to drying are reversible. For example, sample LiAlCl_6 heated at 200°C for 9 h yields a spectrum (not shown) identical to those of LiAlCl_5 at $\text{RH} = 0\%$ (Figure 1e) and heated at 200°C for 2 h (Figure 1f). After rehydration for 12 h over a $\text{RH} = 84\%$ salt buffer, the LiAlCl_6 sample yields spectra similar to those of the paste (compare parts g and n of Figure 1 with parts a and h). The spectra for the LiAlCl_6 sample are slightly broadened due to paramagnetic effects related to the 0.1% Fe^{3+} that was added in this sample to increase the ^{29}Si relaxation rate of silicate LDHs prepared using it in a different study.¹⁰ Spectra taken at the higher H_0 field of 17.6 T ($\nu_0 = 73.5\text{ MHz}$ for ^{35}Cl , sample LiAlCl_8 , Figure 2) confirm these observations. As noted above, the singularities for the CSA-dominated resonances of the fully dehydrated samples remain unchanged, but the structureless resonance narrows in both the static and MAS spectra, and its peak maxima shift to more positive values relative to those at $H_0 = 11.7\text{ T}$. These observations clearly indicate the presence of some quadrupolar contribution to this resonance. Simulation of the static room humidity spectrum (Figure 2b) yields the same ratio ($0.65/0.35$) of the two components as obtained from the low field spectrum. As at $H_0 = 11.7\text{ T}$, the MAS peak for this resonance is not reduced as much as expected (either to very narrow peaks if the quadrupolar contribution is small or by ca. $2/3$ if it dominates), suggesting the presence of a range of local structural environments and partial averaging due to dynamical effects. The 0 ppm

feature of the static paste spectrum (Figure 2a) is again due to surface Cl^- under fast exchange with solution-like sites.

Interlayer Cl^- Dynamics: Variable Temperature

^{35}Cl NMR. The variable-temperature, static ^{35}Cl NMR spectra (Figure 3) of a paste sample of LiAlCl_5 provide important insight into the interlayer dynamics suggested by the room-temperature NMR data and demonstrate that the surface Cl^- and interlayer Cl^- have significantly different dynamical behaviors. At -90°C , the spectrum contains only a single, broad, featureless peak skewed to the right, indicating a disordered structure, a dominantly triaxial local symmetry at Cl^- and significant second-order quadrupolar contribution to the line shape. This peak is very similar to that observed for $\text{Cl}^-\text{Mg,Al}$ hydrotalcite and Friedel's salt (the $\text{Cl}^-\text{Ca}_2\text{Al}$ LDH) at the same temperature⁴ and indicates rigidly held chloride. With increasing temperature, a sharp solution-like peak at ~ 0 ppm first occurs at -60°C , indicating onset of dynamical exchange of surface Cl^- with solution-like sites. This component is present up to 100°C . Appreciable narrowing of the broad peak begins by -30°C , and at 18 and 40°C , all three components present in the room-temperature spectra are resolved. At 70°C , the relative intensity of the CSA-dominated component is greatly reduced, and at 100°C the spectrum contains only the solution-like peak and a symmetrical resonance about 80 ppm broad at half-height.

The observed peak narrowing and change from triaxial to uniaxial symmetry at below-zero temperatures is very similar to our previous observations for interlayer Cl^- in Mg,Al hydrotalcite and Friedel's salt.⁴ For those phases the changes are due to a dynamical order-disorder phase transition involving a change from rigidly held interlayer water and anions to rapid ($> 10^5\text{ Hz}$) hopping librational motion of interlayer water molecules among different hydrogen-bonding configurations.^{4,7} Molecular dynamics simulations of the Mg,Al and Ca,Al compounds show that this libration occurs at frequencies on the order of 10^{11} Hz (ca. $350\text{--}450\text{ cm}^{-1}$ in IR and Raman spectra). It is readily observable in far-IR spectra for the Mg,Al , Ca,Al , and Li,Al phases.²⁶ At low temperature, the hydrogen bond network is statistically disordered leading to the ^{35}Cl NMR spectrum observed at -90°C , whereas above the phase transition the rapid librational hopping leads to time-averaged uniaxial symmetry at $^{35}\text{Cl}^-$. XRD observations¹⁷ and MD results described below indicate that for the Li,Al compound, the H-bonds between the interlayer waters and Cl^- are in the plane of the Cl^- , whereas in the Mg,Al and Ca,Al compounds they are at $\sim 50^\circ$ to the plane due to displacement of the water molecules from the center of the interlayer.⁷ Nonetheless, restricted libration plays an important role in creating the observed peak narrowing for all these phases.

The loss of the uniaxial component and the peak narrowing observed at 70 and 100°C is also a dynamical effect, but is due to exchange (hopping) of Cl^- among the interlayer sites. This site exchange is similar in

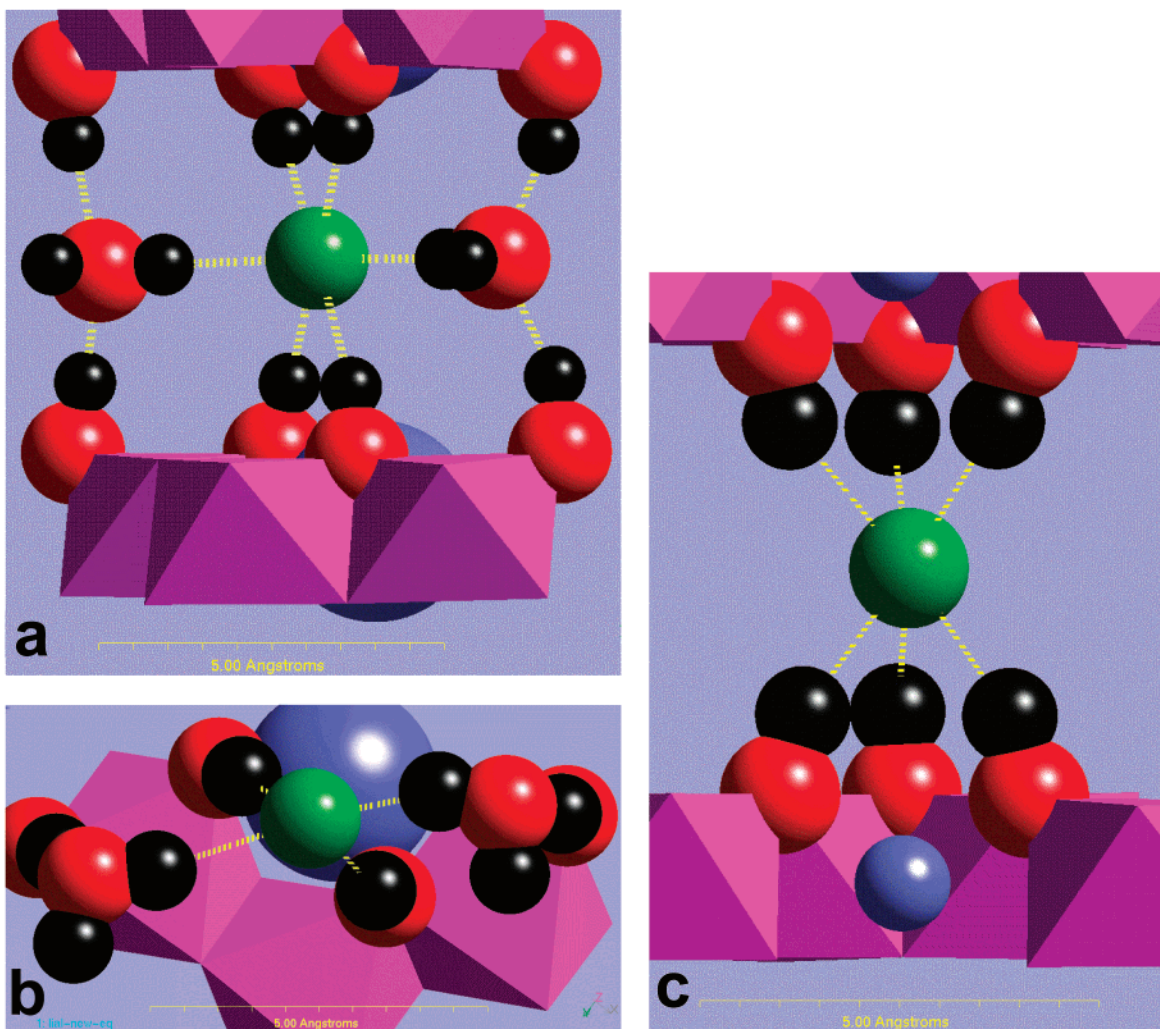


Figure 5. Representative schemes of Cl⁻ and H₂O environments in the interlayer of LiAl₂(OH)₆Cl·H₂O. Cl⁻ ion located in a distorted octahedral environment viewed from the direction parallel (a) and perpendicular (b) to the interlayer, respectively. Side view (c) of a Cl⁻ ion in a trigonal prismatic environment of OH groups for dehydrated phase. Green balls = Cl⁻, red balls = O of water or OH, black balls = H of water or OH, pink octahedron = Al of hydroxide layer, and blue balls = Li of hydroxide layer (shown not to scale to improve visibility in parts a and b).

many ways to that observed for Cs⁺ in smectite clays.^{27,28} Because of complications due to site overlap and quadrupolar effects, it is not possible to unambiguously determine the frequencies of this motion or its temperature dependence,^{5,6} but at 70 °C this frequency must be at least on the order of the peak width at 40 °C, ~10³ Hz. Comparable site hopping occurs for the Mg,Al and Ca,Al compounds,⁴ but because there is only one spectroscopically resolvable interlayer Cl⁻ site in these compounds, it results in only peak narrowing. This rapid interlayer site hopping is consistent with the easy synthesis of this phase by transformation from crystalline gibbsite.^{10,29}

The different temperature dependences of the dynamics of the interlayer and surface Cl⁻ must be due to differences in their interaction with the hydroxide layer and steric restrictions. The surface Cl⁻ has less electrostatic interaction with the positive charge of the hydroxide layer and fewer spatial restrictions. Thus,

observable dynamics for it begins at a lower temperature. It is surrounded on one side by only water molecules, allowing rapid exchange with fully hydrated, solution-like sites near the surface. Molecular dynamics simulations show that for Friedel's salt the exchange occurs at frequencies on the order of 10¹⁰ Hz with bulk water present,⁷ and because its layer charge is similar to that of the LiAl₂ compound the exchange frequencies here are probably similar. In contrast, interlayer Cl⁻ is electrostatically attracted to hydroxide layers on both sides and its motion is restricted to within the layer.

Interlayer Cl⁻ Sites: NMR, Molecular Dynamics Calculations and Diffraction. Comparison of the NMR results, molecular dynamics (MD) calculations, and previously published diffraction results¹⁷ provides important new insight into the interlayer structure and dynamics of the Cl-LiAl₂ phase. The structure of fully hydrated LiAl₂(OH)₆Cl·H₂O based on Rietveld refinement of powder neutron diffraction data demonstrate a highly disordered Cl⁻ and water distribution in the interlayer.¹⁷ As noted above, the broad and skewed ³⁵Cl NMR spectrum observed at -90 °C is fully consistent with this interpretation. In contrast, the single, sym-

(27) Weiss, C. A.; Kirkpatrick, R. J.; Altaner, S. P. *Geochim. Cosmochim. Acta* **1990**, 54, 1655–1669.

(28) Weiss, C. A.; Kirkpatrick, R. J.; Altaner, S. P. *Am. Mineral.* **1990**, 75, 970–982.

(29) Fogg, A. M.; O'Hare, D. *Chem. Mater.* **1999**, 11, 1771–1775.

metric peak observed at 100 °C is indicative of dynamical averaging of the signal from $^{35}\text{Cl}^-$ on all sites present. The two resolvable spectral components for interlayer Cl^- near room temperature, however, suggest the presence of two dynamically different types of interlayer Cl^- sites near room temperature. The Fourier maps for the interlayer region based on the diffraction data show no evidence of localization of the Cl^- or water molecules on lattice sites, although the data can be fit with five Cl^- and five interlayer O sites.¹⁷

The results of the MD calculations for the $\text{LiAl}_2(\text{OH})_6\text{Cl}\cdot\text{H}_2\text{O}$ phase provide important insight into these structural and dynamical observations. The computational results are illustrated by the contour plots of the atomic probability densities in the plane of the interlayer averaged over the 100 ps of the MD run shown in Figure 4. Dynamically, the computations show the expected rapid (ca. 10¹¹ Hz) librational hopping of the water molecules among possible H-bonding orientations and also relatively rapid hopping of Cl^- and water molecules among sites. The restricted libration of the water molecules is comparable to that observed for interlayer water in other LDH compounds^{7,8} and is well illustrated by the multiple peaks for the H atoms of individual water molecules in the probability density contour plot. The calculated mean frequency of Cl^- site hopping is on the order of 3×10^8 Hz, and that for water about an order of magnitude faster. Although these values are near the limits of statistical reliability for the calculations, they are fully consistent with the observed peak narrowing in the variable-temperature ^{35}Cl NMR data above. The minimum hopping frequency from these data is on the order of 10³ Hz.

Structurally, the results indicate a disordered but not random interlayer arrangement. The water molecules are located at the center of the interlayer along the c-direction, as also shown by the diffraction data,¹⁷ and are predominantly located near the H atoms of the OH groups. The O atoms of the waters on these positions receive two H-bonds, one each from an OH group on either side of the interlayer. Because of the eclipsed layer stacking,¹⁷ the water molecules are in a stable, distorted tetrahedral coordination (Figures 5a,b) very similar to that in bulk liquid water.³⁰ This configuration also allows the H atoms of the water molecules to be predominantly in the center of the interlayer, where they can make H-bonds to the Cl^- . The Cl^- atoms occupy several types of sites, all of which are at the center of the interlayer along the c-axis. A few are near the vector between Li atoms in adjacent hydroxide layers. These sites are comparable to the Cl^- sites in the dehydrated phase, although the Cl^- in the hydrated phase is rarely exactly along the Li–Li vector. Others are in the trigonal prisms of OH groups between vacant tetrahedral sites of adjacent hydroxide layers (Figure 5c). For both of these sites, the Cl^- is 6-coordinated by three OH groups from above and three from below in a trigonal prism arrangement. Most Cl^- ions, however, are on distorted octahedral sites formed by H-bonds from two OH groups above, two OH groups below, and one H atom of two different water molecules (Figure 5a,b). The four OH groups of this site form a rectangle

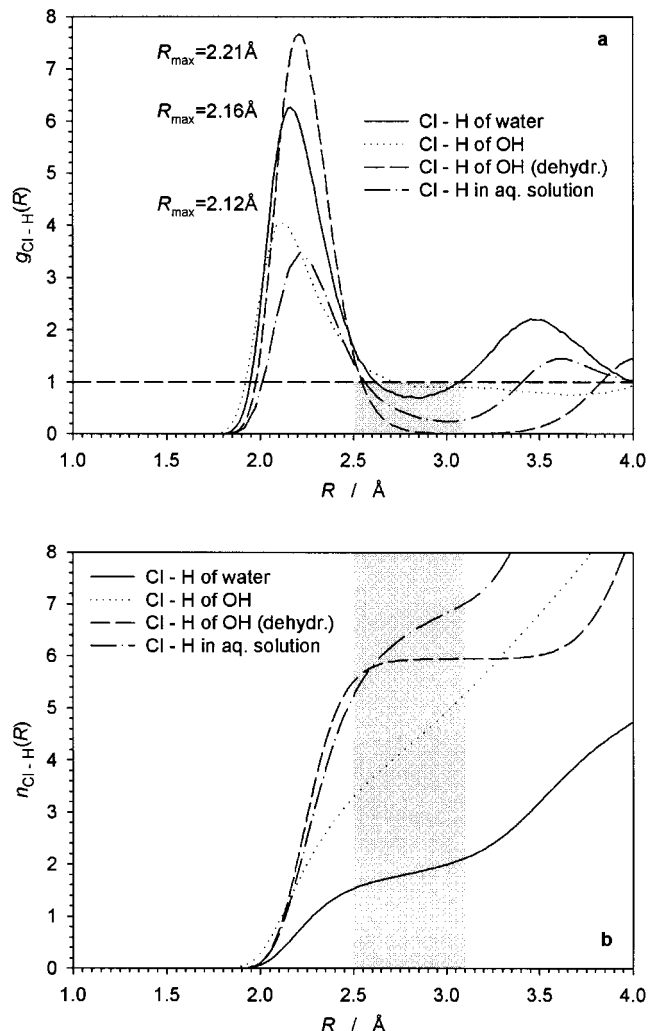


Figure 6. Radial distribution functions (a) and integrated nearest-neighbor coordination numbers (b) for interlayer Cl^- and H in $\text{LiAl}_2(\text{OH})_6\text{Cl}\cdot\text{H}_2\text{O}$ computed using MD methods. Simulation results for Cl^- in 1.1M NaCl aqueous solution at ambient conditions are shown as dash-dotted lines for comparison. Gray regions indicate the range of Cl^- – H distances around the first minimum of $g_{\text{Cl}-\text{H}}(R)$ that can be reasonably used as a cutoff threshold for the formation of Cl^- – H hydrogen bonds.

due to the eclipsed layer stacking, and the mean Cl^- position is near its center. The H-bonds from the two water molecules are on an axis ca. 60° to the square of OH groups, and the octahedron is quite asymmetric and also dynamic due to the hopping libration of the water molecules.

This structural arrangement and its similarity to that of Cl^- in aqueous solution are well illustrated by the computed radial distribution functions shown in Figure 6. In the interlayer, each Cl^- receives on average about 2 H-bonds from interlayer water molecules and 4 from OH groups of the main layers. The modal H-bond distances to Cl^- are 2.12 Å for the waters and 2.16 Å for the OH groups. These coordination numbers and H-bond distances are very similar to those in dilute aqueous solutions at room temperature and 1 bar pressure. For 1.1 M NaCl solution, MD calculations using the same methods show that the mean number of H-bonds to Cl^- is 6.5, and the mean H-bond distance is 2.22 Å, in good agreement with experimental data³¹

and previous simulations.²⁴ Support for the accuracy of the MD calculations comes from the excellent agreement between the observed and computed unit cell dimensions: $a = 5.096$ vs 5.200 Å, $b = 5.096$ vs 5.200 Å, and $c = 15.292$ vs 15.340 Å for observed and computed values, respectively.¹⁷ In addition, the initial eclipsed layer stacking remains stable throughout the simulation, even though it was not restricted to do so. The resulting calculated unit cell angles, $\alpha = 90.18^\circ$, $\beta = 89.94^\circ$, and $\gamma = 120.00^\circ$, are in good agreement with the observed hexagonal symmetry of the system.¹⁷

The computed interlayer structure also provides an explanation for the unusual maximum 1/1 H₂O/Cl ratio for many of the LiAl₂ LDHs. Other well-ordered LDH phases, most notably Friedel's salt (CaAl₂), have maximum H₂O/Cl ratios of 2. For Friedel's salt, however, the O atoms of the water molecules coordinate the large cation Ca of the hydroxyl layer^{7,15} and thus form two sublayers on either side of the center of the interlayer along the *c*-axis. The Cl⁻ are, thus, at any instant 10 coordinate (six OH and four water molecules), there is a stable but dynamical H-bonding network, and the H-bonds from the OH groups are given predominantly to the Cl⁻. Molecular dynamics modeling for the Cl⁻-Mg,Al LDH suggest a similar but less ordered arrangement with at least some of the O atoms of water molecules coordinating Mg.⁸ In contrast, in the LiAl₂ phases, the O atoms of the waters cannot coordinate either Li or Al, occur in the center of the interlayer along the *c*-axis, and are stabilized by the H-bonding network. Of the six OH groups per formula unit, two are used to coordinate the one water and four to coordinate the one Cl⁻. Thus, there are no stable sites for substantial amounts of additional water. Indeed, in an MD simulation with a H₂O/Cl ratio of 2/1, the structure disaggregated.

These computed results are in excellent agreement with experimental water vapor absorption and RH-controlled XRD results.³² These data show that LiAl₂-(OH)₆Cl⁻*n*H₂O sorbs 5.2 wt % water in the relatively low and narrow RH range from 3% to 30% but that in the same RH range its basal spacing increases only from 7.36 to 7.67 Å. The change in the Cl⁻ environment with changing relative humidity observed by ³⁵Cl NMR for LiAl₂(OH)₆Cl⁻*n*H₂O contrasts with our previous results for the nonswelling LDHs. For the NO₃⁻ and SeO₃²⁻-MgAl LDH phases there is no significant interlayer water sorption, no swelling, and no change in the interlayer anion environments.^{5,6} Clearly, the contrasting interlayer water environments in the LiAl₂ and

Mg,Al LDHs play a critical role in determining the relationship between the water sorption and swelling behavior.

For the ³⁵Cl NMR results, the computed interlayer structure suggests that the resonance dominated by CSA near room temperature is due to Cl⁻ on the two prism sites and the structureless peak to Cl⁻ on the distorted octahedral sites. Both trigonal prism sites have the required time averaged uniaxial symmetry. In the simulations, 8/32 Cl⁻ appear to be on these sites, in surprisingly good agreement with the observed 0.23 relative intensity of the CSA-dominated site for the paste sample. The distorted octahedral sites are highly asymmetric at any instant, but the combination of water libration and Cl⁻ and water site hopping leads to the observed peak narrowing. The observation of separate NMR resonances for these sites near room temperature and their merger at higher temperatures demonstrates that exchange between them is not occurring at frequencies greater than ca. 10⁴ Hz at room temperature and that the frequency of exchange increases to ca. 10⁴ Hz near 70 °C.

The MD results of the dehydrated phase are in excellent agreement with the structure determined from the diffraction data.¹⁷ In the minimum energy configuration, the Cl⁻ occupy positions in the center of the interlayer and on the vector between Li atoms of adjacent layers (chain sites), and the layer stacking has the eclipsed arrangement, as observed in the diffraction studies.¹⁷ The unit cell dimensions are also in good agreement with $a = 5.100$ vs 5.177 Å, $b = 5.100$ vs 5.177 Å, and $c = 14.299$ vs 14.765 Å for observed¹⁷ and simulated values, respectively. In a simulation that started with the configuration of the hydrated phase but with the water molecules removed, the Cl⁻ rapidly moved to the Cl⁻...3OH⁻...Li⁺...3OH⁻...Cl chain sites and remained there throughout the run. The unconstrained simulation cell maintained its hexagonal symmetry to even a higher degree than for the hydrated phase simulations (calculated $\alpha = 90.01^\circ$, $\beta = 89.99^\circ$, $\gamma = 120.00^\circ$).

Acknowledgment. This research is supported by NSF Grant EAR 95-26317 and DOE Grant DEFG02-00ER15028, R.J.K.P.I. We would like to thank Dr. David L. Bish for help with collecting XRD data under controlled relative humidity (RH) and Dr. Shan-li Wang for water sorption measurements. The computations were supported by the National Computational Science Alliance (Grant EAR 990003N), utilizing NCSA SGI/CRAY Origin2000 computers and the Cerius2-4.0 software package from Molecular Simulations Inc.

(31) Powell, D. H.; Neilson, G. W.; Enderby, J. E. *J. Phys. Condens. Matter* **1993**, *5*, 5723.

(32) Hou, X.-Q.; Bish, D. L.; Wang, S.-L.; Johnston, C.; Kirkpatrick, R. J. *Am. Mineral.*, submitted for publication.